

TARGET CLASSIFICATION WITH LOW-RESOLUTION SURVEILLANCE RADARS BASED ON MULTIFRACTAL FEATURES

Q. S. Li^{1, 2 *} and W. X. Xie¹

¹Institute of Intelligent Information, Shenzhen University, Shenzhen 518060, China

²School of Physics and Electronic Information, Gannan Normal University, Ganzhou 341000, China

Abstract—The multifractal characteristics of return signals from aircraft targets in conventional radars offer a fine description of dynamic characteristics which induce the targets' echo structure; therefore they can provide a new way for aircraft target classification and recognition with low-resolution surveillance radars. On basis of introducing the mathematical model of return signals from aircraft targets in conventional radars, the paper analyzes the multifractal characteristics of the return signals as well as the extraction method of their multifractal features by means of the multifractal analysis of measures, and puts forward a multifractal-feature-based classification method for three types of aircraft targets (including jet aircrafts, propeller aircrafts and helicopters) from the viewpoint of pattern classification. The analysis shows that the conventional radar return signals from the three types of aircraft targets have significantly different multifractal characteristics, and the defined characteristic parameters can be used as effective features for aircraft target classification and recognition. The results of classification experiments validate the proposed method.

1. INTRODUCTION

Most of active surveillance radars adopt the conventional low-resolution radar system. If they are able to provide target attribute information such as its class, model, etc. while detecting a target, they certainly will have important practical significance for the aerial

Received 15 September 2012, Accepted 30 October 2012, Scheduled 1 November 2012

* Corresponding author: Qiusheng Li (bjliqiusheng@163.com).

defence of a country. Comparing with the working of low-resolution searching plus high-resolution recognition, if we can introduce a function of target classification and recognition into a low-resolution radar, and realize simple target classification and recognition directly by means of signal processing in most active surveillance radars, then we can avoid the increase of system cost and complexity brought by the broadband rebuilding. Nowadays, most active surveillance radars achieve their limited target classification and recognition abilities by a recognition method based on the experience and tactics, and it is up to the radar operators to distinguish the class and sortie of aircraft targets according to echo intensity as well as its undulation characteristics, target motion characteristics, identification friend or foe (abbr. IFF) signals, etc., so it is difficult to meet the need of modern information wars. Therefore, seeking a feasible target classification and recognition method with low-resolution radars has long been an important research aspect in the realm of radar target recognition, and the research has a wide application prospect. However, due to the low-resolution radar system, such as low pulse repetition frequency (abbr. PRF), narrow signal band, short irradiation time, automatic target classification and recognition with low-resolution radars also becomes a research difficulty [1–3].

So far, the features extracted in methods with respect to target classification and recognition with low-resolution radars can be divided into two kinds in principle: one kind of features is extracted based on the target RCS, echo amplitude undulation, echo phase undulation, target motion parameters, echo vision effect or its 2-D gray-level map, etc. [4–7]; the other kind of features is extracted based on the jet engine modulation (abbr. JEM) features generated by target rotating parts, such as the rotor, empennage, propeller, turbine fan, etc. [8–14]. JEM modulation features are determined by the leaf number and rotary speed of the rotating parts of a target and independent with the target attitude angle if no LOS-sheltering, i.e., the rotating parts can be seen by the radar. Now proposed extraction methods for JEM features mainly contain the complex cepstrum method, self-correlation method, AR model power spectrum method, SVD eigenvalue decomposition method, etc., but most of these methods have high computational complexity, and often demand a higher PRF and longer observation time, so it is difficult to apply them to engineering [3].

Actually, as a kind of complex target, the size of an aircraft is generally far longer than the wavelength of conventional radars, so the echo scattering of aircraft targets is in the optical area, which means that the general target scattering echo is the linear superposition of the scattering echo from each independent scattering center, and the

echo undulation reflects the complex micro-motion modulation effect of various parts of an aircraft target and contains target information such as the fine geometry structure, material composition, etc. If these nonlinear modulation features which reflect the physical characteristics of an aircraft target can be extracted effectively, then we can directly apply them to the classification and recognition of different types of aircraft targets. As we all know, fractal is an important nonlinear research method. If one performs the multifractal analysis of measures on radar return signals from an aircraft target, it is hopeful to reveal the nonlinear dynamic characteristics which induce the echo structure as well as their relationships with the target structure [15, 16].

Based on the above analysis, the paper plans to analyze the multifractal characteristics of the conventional radar return signals from aircraft targets by means of the multifractal analysis of measures, and puts forward a multifractal-feature-based method for aircraft target classification so as to classify three types of aircraft targets (including jet aircrafts, propeller aircrafts and helicopters) in condition of no compensation for airframe components from the viewpoint of pattern classification. Firstly, on basis of introducing the mathematic model of conventional radar return signals from aircraft targets as well as the ideal JEM features, the paper points out that it is difficult to extract the JEM features in the low-resolution radar system due to low PRF, short irradiation time, etc. Secondly, on basis of introducing the multifractal theory, the paper analyzes the multifractal characteristics of return signals from aircraft targets in condition of low PRF and short irradiation time by the multifractal analysis of measures, proposes a multifractal-parameter-based feature extraction method, and defines four characteristic parameters to lower the dimension of the eigenvector for target classification. Finally, aiming at the proposed classification method, the paper takes the support vector machine (abbr. SVM) as the classifier to do classification experiments and takes the eigenvalue-spectra-dispersion-based method proposed in [3] as a contrast to analyze the algorithmic performance and validate the validity of the proposed method.

2. ECHO MATHEMATIC MODEL OF AIRCRAFT TARGETS

Despite the ground clutter and other electronic jamming, a conventional radar return signal from an aircraft target should include the airframe section, echo section of the rotating parts (i.e., the JEM section), and noise section [17], viz.

$$s(t) = a_s(t) [C_a s_a(t) + C_{\text{jem}} s_{\text{jem}}(t)] + C_n s_n(t), \quad (1)$$

where $a_s(t)$ denotes the comprehensive impact of the radar system on the return signal, equivalent to $a_s(t) = a_t(t)a_a(t)a_r(t)$. $a_t(t)$ is the transmission signal model, $a_a(t)$ the antenna scan and receiving model, and $a_r(t)$ the receiver model. $s_a(t)$, $s_{\text{jem}}(t)$ and $s_n(t)$ denote the airframe section, JEM section, and noise section respectively. C_a , C_{jem} and C_n denote the intensity coefficients of the airframe section, JEM section, and noise section respectively.

Concretely, if we assume that there is an aircraft target containing M engines, located in the far field of the radar with the distance R_0 , azimuth α , and elevation β , then during the brief time when the aircraft is exposed to the irradiation of the radar, the fundamental frequency airframe section is [3]

$$s_a(t) = \exp(j2\pi f_d t + j4\pi R_0/\lambda), \quad (2)$$

where λ is the wavelength of the radar; $f_d = 2u/\lambda$ denotes the airframe Doppler frequency. u is the projection of the airframe velocity in the radar-target LOS, i.e., $u = u_f \cos \varphi$, u_f the flying velocity of the aircraft, and φ the inclination of u_f relative to the radar-target LOS. The fundamental frequency JEM section is [11]

$$\begin{aligned} s_{\text{jem}}(t) = & \exp\left(j2\pi f_d t + j\frac{4\pi R_0}{\lambda}\right) \sum_{m=0}^M v(\alpha, \beta', P) \\ & \cdot \sum_{k=0}^{N_m-1} [g_{1m} + g_{2m} \cos(\theta_{km} + \omega_{rm}t - \alpha)] \\ & \cdot (L_{2m} - L_{1m}) \operatorname{sinc}\left[\frac{2\pi}{\lambda} (L_{2m} - L_{1m}) \cos\beta' \cos(\theta_{km} + \omega_{rm}t - \alpha)\right] \\ & \cdot \exp\{j4\pi/\lambda\} \cdot \left[\frac{L_{1m} + L_{2m}}{2} \cos\beta' \cos(\theta_{km} + \omega_{rm}t - \alpha)\right] \quad (3) \end{aligned}$$

where $v(\alpha, \beta', P)$ is the visibility function, used to describe the LOS-sheltering problem of the rotating parts. P denotes some concrete aircraft type, $\beta' = \beta$ when the rotating plane is parallel to the flight path, $\beta' = \pi/2 - \beta$ when the rotating plane is vertical to the flight path; N_m , ω_{rm} , L_{1m} and L_{2m} are the leaf number, rotary speed, distance from the oar rootage, and oar tine to the oar center of the m th group of rotating parts respectively; $\theta_{km} = \theta_0 + 2\pi k/N_m$, $k = 0, 1, \dots, N_m - 1$, where θ_0 is the initial phase of the 0th oar leaf. If we ignore the torsion of oar leaves and use θ_m to stand for the leaf angle, then we have $g_{1m} = \sin(|\beta'| + \theta_m) + \sin(|\beta'| - \theta_m)$, $g_{2m} = \operatorname{sign}(\beta')[\sin(|\beta'| + \theta_m) - \sin(|\beta'| - \theta_m)]$.

The Fourier transform of Equation (3) is given by [11]

$$S_{\text{jem}}(f) = \sum_{m=0}^M v(\alpha, \beta', P) \sum_{k=-N_{1m}}^{N_{1m}} c_{m,k} \delta(f - f_d - kf_{Tm}), \quad (4)$$

i.e., the modulation spectrum is made up of a series of linear spectrum. With respect to the m th group of rotating parts, the interval of adjacent spectrum lines is $f_{Tm} = N_m \omega_{rm} / 2\pi$, determined by N_m and ω_{rm} ; the spectrum line amplitude $C_{m,k}$ is determined by parameters N_m , λ , β' , L_{1m} , L_{2m} and θ_0 together with the Bessel function; N_{1m} is the number of spectrum lines of one sideband. N_{1m} and B_{1m} (the bandwidth of one sideband) can be written as [11]

$$N_{1m} = 8\pi L_{2m} \cos \beta' / (N_m \lambda) \quad (5)$$

and

$$B_{1m} = 4\omega_{rm} L_{2m} \cos \beta' / \lambda. \quad (6)$$

Currently, the research work on the extraction of JEM features is mainly concentrated on estimating the interval of adjacent spectrum lines [8–14, 17–25]. However, in the conventional low-resolution radar system, the radar irradiation time towards a target is very short (often 20~30 ms), and PRF is very low (often a few hundred ~ a few thousand Hz), so the resolution power in the Doppler domain is lower, and the return signals from different types of aircraft targets are often overlapped in the Doppler domain. Thus, for low-resolution surveillance radars with lower PRF and shorter irradiation time, it is very hard to estimate the interval of adjacent spectrum lines, and it is also very difficult to estimate the bandwidth of one sideband [3]. Below we will analyze the multifractal characteristics of return signals from three types of aircraft targets (including jet aircrafts, propeller aircrafts and helicopters), and discuss the feature extraction method propitious to the classification of these three types of aircraft targets.

3. EXTRACTION METHOD OF MULTIFRACTAL FEATURES

Since Mandelbrot introduced the concept of fractal geometry in the seventh decade of the 20th century, fractal theory has been widely applied to many subjects and technical realms such as natural science, social science, engineering, etc. However, with the development of the theoretical and applied research, people gradually wake up to the fact that for a great deal of objective fractal objects, it is difficult to depict their fine structure only by a single fractal dimension. Therefore, Grassberger [26], Hentschel and Procaccia [27], and Halsey

et al. [28] put forward multifractal theory systematically at the beginning of the eighth decade of the 20th century and introduced the generalized dimension and multifractal spectrum to describe a fractal object. Owing to considering the spatial singularity distribution of a fractal object in geometrical subsets, multifractal theory has been rapidly applied to almost all realms concerning fractal such as onflow, earthquake, etc. Now, multifractal has become an important research means for complex nonlinear systems.

3.1. Multifractal Model

What multifractal describes is the characteristics of different levels of a fractal object during the growing process. Therefore, we can divide the investigated object into several small regions, noting the total number of the regions and the size of a region with N and ε ($\varepsilon < 1$) respectively, and let the growth probability of the growth interface of the fractal object be $P_i(\varepsilon)$. Generally, there are different growth probabilities in different regions, and the growth probabilities of different regions can be expressed by different indexes σ , i.e., [26]

$$P_i(\varepsilon) \propto \varepsilon^\sigma, \quad i = 1, 2, \dots, N. \quad (7)$$

If the values of σ for all the regions are the same, then the investigated object is a mono-fractal object; contrarily, if the values of σ for different regions are different, then the investigated object is a multifractal object. Constructing a subset with small regions with the same σ , then due to $\varepsilon < 1$, it can be seen that the maximum index σ_{\max} corresponds to the minimum probability subset, while the minimum index σ_{\min} corresponds to the maximum probability subset. Let the number of small regions with the same σ be $N_\sigma(\varepsilon)$, then we have [26]

$$N_\sigma(\varepsilon) \propto \varepsilon^{-f(\sigma)} \quad (\varepsilon \rightarrow 0), \quad (8)$$

where σ is called local fraction-dimension, or singular index, whose value reflects the size of the growth probability in a small region; $f(\sigma)$ denotes the fractal dimension of the subset with the same σ . Because of the large number of small regions, we can use an infinite serial $f(\sigma)$ corresponding to different σ to represent the fractal dimensions of the whole fractal object; therefore, $f(\sigma)$ is called multifractal spectrum. The $\sigma - f(\sigma)$ curve reflects the distribution features of the growth probabilities.

3.2. Calculation of Multifractal Spectrum

Multifractal objects may be divided into two kinds: regular multifractal and irregular multifractal. Generally speaking, we can

calculate their multifractal spectrum by statistic physics methods. Therefore, firstly we define a partition function [28]

$$\Gamma(q, \varepsilon) = \sum_{i=1}^N P_i^q(\varepsilon) = \varepsilon^{\tau(q)}, \tag{9}$$

where, $q \in (-\infty, +\infty)$, but we can determine its range according to the actual circumstances. If the right equation of Equation (9) is tenable, i.e., the partition function takes on a power function relationship with ε , then from the slope of the $\ln \Gamma(q, \varepsilon) - \ln \varepsilon$ curve we can get $\tau(q)$, which is often called mass index. q and $\tau(q)$ are also a group of parameters using to describe multifractal. If $\tau(q)$ is a linear function of q , then the fractal object is a mono-fractal object; however, if $\tau(q)$ is a convex function of q , then the fractal object is a multifractal object.

If $q \gg 1$, then the subsets with large probabilities will dominate in $\sum P_i^q(\varepsilon)$. If $q \ll -1$, then the subsets with small probabilities will dominate in $\sum P_i^q(\varepsilon)$. Therefore, we can carry out a fine study on the internal structure of a fractal object by weighted processing.

In order to derive $f(\sigma)$ from the relationship between $\tau(q)$ and q , at first we introduce the generalized fractal dimension D_q [26, 27]:

$$D_q = \frac{\tau(q)}{q-1} = \frac{\ln \Gamma(q, \varepsilon)}{(q-1) \ln \varepsilon} \quad (\varepsilon \rightarrow 0). \tag{10}$$

Obviously, D_q has different senses for different values of q , e.g., D_0 is the simple fractal dimension when q equals 0; D_1 is the information dimension when q equals 1. Equation (9) can be rewritten as [27]

$$\Gamma(q, \varepsilon) = \sum_{i=1}^N P_i^q(\varepsilon) = \sum N(P) P^q, \tag{11}$$

i.e., we can calculate $\sum P_i^q(\varepsilon)$ through grading the regions according to their growth probabilities, where $N(P)$ denotes the number of the regions with the same growth probability P . Substitute Equations (7) and (8) into (11), then (11) can be expressed as [27]

$$\Gamma(q, \varepsilon) = \sum \varepsilon^{\sigma q - f(\sigma)} = \varepsilon^{\tau(q)}. \tag{12}$$

Rewrite the right equation of Equation (12) as [27]

$$\sum \varepsilon^{\sigma q - f(\sigma) - \tau(q)} = 1. \tag{13}$$

Evidently, when $\varepsilon \rightarrow 0$, those items with $\sigma q - f(\sigma) - \tau(q) > 0$ will verge on zero, while those items with $\sigma q - f(\sigma) - \tau(q) < 0$ will be impossible. Otherwise, the sum will become infinite. Consequently, only those items with $\sigma q - f(\sigma) - \tau(q) = 0$ will be kept, i.e., [27]

$$f(\sigma) = \sigma q - \tau(q), \tag{14}$$

and σ can be obtained by the differential coefficient of $\tau(q)$ on q , i.e., [27]

$$\sigma = d\tau(q)/dq. \quad (15)$$

From Equations (14) and (15), we can see that the relationship among $\tau(q)$, q and $f(\sigma)$, σ is the Legendre Transform, i.e., one can get the multifractal spectrum $f(\sigma)$ by the Legendre Transform of $\tau(q)$ and q .

Table 1. The structure parameters and rotary speeds of twenty-five aircrafts belonging to three types.

Aircraft number	Number of blades	L_1/m	L_2/m	Rotary speed/rpm
J-A	38	0.38	1.1	3520
J-B	27	0.18	0.51	8615
J-C	30	0.3	1	3000
J-D	33	0.2	0.6	5000
J-E	42	0.24	0.8	4000
J-F	50	0.3	0.9	3500
P-A	4	0.68	1.7	1200
P-B	4	0.79	1.95	1245
P-C	3	0.27	0.76	3400
P-D	3	0.23	0.66	3400
P-E	3	0.23	0.66	2340
P-F	2	0.12	0.33	6060
P-G	2	0.12	0.33	7010
P-H	2	0.12	0.33	7400
P-I	2	0.12	0.33	7800
H-A	5	0	10.645	192
H-B	5	0	8.6	242
H-C	8	0	16	132
H-D	4	0	7.8	217
H-E	4	0	5.5	384
H-F	4	0	5.335	395
H-G	3	0	5	406
H-H	3	0	5.345	394
H-I	2	0	7.31	324
H-J	2	0	5.64	394

*Note: J — Jet aircrafts, P — Propeller aircrafts, H — Helicopters.

3.3. Extraction of Multifractal Spectrum Features

According to Equation (1), return signals from aircraft targets should include the airframe section, JEM section, and noise section. We will simulate the radar echo data of the three types of aircraft targets according to Equations (1)–(3). The aircraft parameters and case parameters are presented by Tables 1 and 2, respectively. For a helicopter, compared with its rotor, its empennage has a lesser leaf diameter and quicker rotary speed. The echo energy of its empennage possesses a smaller ratio in the general echo energy, so its JEM section is mainly affected by its rotor. During the simulation, we set the diameter of the empennage as one third of that of the rotor and the rotary speed of the empennage as three times of that of the rotor, and give them a random rotation angle difference. Both jet aircrafts and propeller aircrafts have two engines, and each of them has a fan with the same structure and rotary speed. Moreover, there is a certain distance and random rotation angle difference between the two fans, and the pitch angle of the oar blades is a random number within a certain range. During the short time when an aircraft is being exposed to the irradiation of the radar, the target can be viewed as a dot moving at a certain speed, so the airframe section is a mono-frequency signal as Equation (2). RCSs of aircraft targets tally with Swerling models, and RCSs of jet aircrafts and those of propeller aircrafts and helicopters tally with Models I and III, respectively. The echo pulses within a scan are correlative. Assume that the radar works at the L -band with its wavelength $\lambda = 0.3$ m and PRF $f_r = 600$ Hz. Figures 1 and 2 show the typical mass index and multifractal spectrum curves of the three types of aircraft targets (The flying attitude can be set randomly) with the observation time T equal to 25 ms and 100 ms, respectively.

It can be seen from Figure 1(a), under condition of $T = 25$ ms, the mass index $\tau(q)$ of return signals from jet aircraft targets is approximatively a linear function of q , so its multifractal characteristic is not distinct; however, $\tau(q)$ of return signals from propeller aircrafts

Table 2. The typical case parameters and flying speeds of three types of aircrafts.

	Distance/km	Height/km	Velocity/m·s ⁻¹
Jets	$U(30, 40)$	$U(15, 23)$	$U(600, 700)$
Propeller aircrafts	$U(30, 40)$	$U(3.95, 12)$	$U(150, 200)$
Helicopters	$U(30, 40)$	$U(0.5, 10)$	$U(56, 98)$

*Note: $U(a, b)$ denotes a uniform distribution in the interval (a, b) .

or helicopters is obviously a convex function of q , which means that their multifractal characteristics are very noticeable. As can be seen from Figure 1(b), under condition of increasing the observation time ($T = 100$ ms), the multifractal characteristics of return signals from jet aircraft targets are still inconspicuous, while those of return signals from helicopter targets strengthen markedly, but the mass index curve of return signals from helicopter targets takes on a different symmetric property from that of return signals from propeller aircrafts. We can see from Figure 2(a) that among the multifractal spectrum curves of return signals from three types of aircraft targets, the range of σ of return signals from jet aircrafts is the smallest, and that of return signals from helicopters takes second place, while that of return signals from propeller aircrafts is the largest, i.e., their echoes present more and more distinct multi-fractal characteristics in turn. Figure 2(b) shows that under the circumstance of increasing the observation time, the range of σ of return signals from jet aircrafts changes very little,

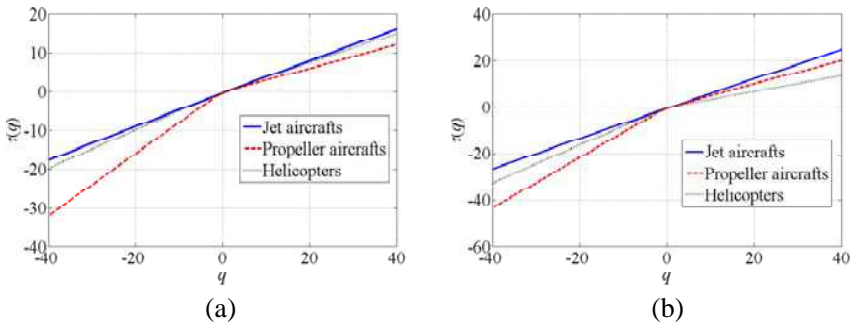


Figure 1. $\tau(q) \sim q$ curves. (a) $T = 25$ ms. (b) $T = 100$ ms.

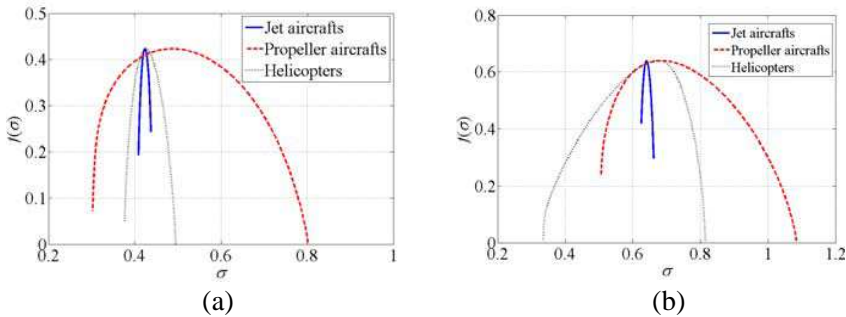


Figure 2. $f(\sigma) \sim \sigma$ curves. (a) $T = 25$ ms. (b) $T = 100$ ms.

while that of return signals from helicopters increases remarkably, but its multifractal spectrum curve has a different symmetric property from that of return signals from propeller aircrafts. Thereinto, the multifractal spectrum of return signals from helicopters is a right-symmetrically campanulate curve, and that of return signals from propeller aircrafts is a left-symmetrically hooked curve. Therefore, Figures 1 and 2 take on corresponding variation characteristics.

We can see from the above analysis that the mass index curves and multifractal spectrum curves of return signals may discriminate these three different types of aircraft targets. Therefore, we define four multifractal characteristic parameters as follows.

1) Mass index symmetric degree

$$R_\tau = \left| \frac{\max \tau(q)}{\min \tau(q)} \right|. \tag{16}$$

2) Spectrum width

$$\Delta\sigma = \sigma_{\max} - \sigma_{\min}. \tag{17}$$

where σ_{\max} and σ_{\min} denote the maximum and the minimum of singular index σ , respectively, corresponding to the minimum probability subset and the maximum probability subset. The size of $\Delta\sigma$ reflects the prominence degree of the multifractal characteristics of the return signal.

3) Difference of the fractal dimensions of the maximum and the minimum probability subset

$$\Delta f = |f(\sigma_{\min}) - f(\sigma_{\max})|. \tag{18}$$

As can be known by [29],

$$f(\sigma_{\min}) - f(\sigma_{\max}) = \frac{\ln(N_{\sigma_{\max}}/N_{\sigma_{\min}})}{\ln \varepsilon}, \tag{19}$$

where $N_{\sigma_{\max}}$ and $N_{\sigma_{\min}}$ are the region numbers of the minimum probability subset and the maximum probability subset, and ε denotes the size of a region. Therefore, the size of Δf reflects the relative distribution proportion of the minimum probability subset and the maximum probability subset.

4) Asymmetric index

$$R_\sigma = \frac{\Delta\sigma_L - \Delta\sigma_R}{\Delta\sigma_L + \Delta\sigma_R}. \tag{20}$$

with

$$\Delta\sigma_L = \sigma_0 - \sigma_{\min}, \tag{21}$$

$$\Delta\sigma_R = \sigma_{\max} - \sigma_0, \tag{22}$$

where σ_0 is the singular index corresponding to the maximum of the multifractal spectrum $f(\sigma)$. It is apparent that R_σ depicts the asymmetric property of the multifractal spectrum curve from the whole.

Figure 3 gives the probability distribution density curves of the four multifractal characteristic parameters of return signals from three types of aircrafts under the previous radar working conditions with the observation time $T = 25$ ms and no compensation for airframe components. As can be seen from the figure, each of the four multifractal features has certain classification abilities. In Figures 3(a) and (b), R_τ and $\Delta\sigma$ can distinguish jet aircrafts from the other two types of aircrafts easily, but they behave badly in the discrimination of propeller aircrafts and helicopters. In Figures 3(c) and (d), Δf and R_σ can discriminate helicopters from the other two types of aircrafts easily; however they are helpless in discriminating propeller aircrafts

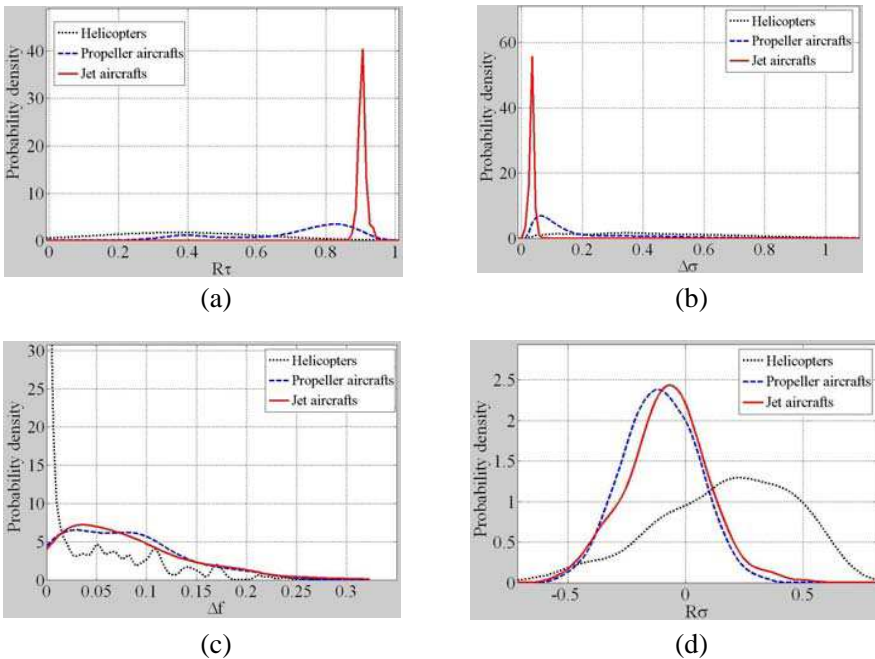


Figure 3. The probability density distribution curves of four multifractal spectrum characteristic parameters. (a) Mass index symmetric degree. (b) Spectrum width. (c) Difference of the fractal dimensions of the maximum and the minimum probability subset. (d) Asymmetric index.

and jet aircrafts. Therefore, if we combine these four characteristic parameters together to classify these three types of aircraft targets, it is hopeful to get a better performance.

4. CLASSIFICATION EXPERIMENTS

According to the aircraft parameters and case parameters shown by Table 1 and 2, respectively, we simulate radar echo data of three types of aircraft targets by Equations (1)~(3) and take them as the experimental data. On basis of analyzing the performance of methods using some typical low-resolution radar target classification features [17–25, 30–32], ref. [3] points out that the classification method based on dispersion situations of eigenvalue spectra (abbr. CMDSES) excels other methods markedly. Therefor, we will take CMDSES as the contrast to analyze the performance of the classification method based on multifractal features (abbr. CMMF) in the following text.

Experiment 1: Take SVM [33] as the classifier to analyze the performance of CMDSES and CMMF contrastively. In the experiment, the classifier takes the Gaussian kernel $K(x_i, x_j) = \exp(-\|x_i - x_j\|^2/\sigma^2)$ as the kernel function. Because there is no prior knowledge about the parameter σ^2 , in the following experiments, we will try different parameter values several times without going beyond the calculation burden and take the parameters which can well classify different types of aircraft targets as the kernel function parameters. All the correct classification rates (abbr. CCRs, here CCR is defined as the ratio of the number of samples which are classified correctly and the total number of samples) given in the following are the classification results using the better kernel function parameters.

Table 3 shows the CCRs of CMDSES and CMMF with the radar operating at *L*-band, PRF $f_r = 600$ Hz, observation time $T = 25$ ms, and signal-to-noise ratio (abbr. SNR) $\text{SNR} = 20$ dB. As can be seen from the table, the average CCR of CMMF is far higher than that of CMDSES whether on training samples or testing samples, and the CCR of each type of aircraft targets is more than approximately eighty-five percent. In addition, CCRs using CMDSES of three types of aircraft targets except jet aircrafts are all lower than those using CMMF, especially the classification performance of CMDSES for helicopters is very low. Consequently, CMMF outstrips CMDSES in the total performance.

Experiment 2: Still take SVM using the Gaussian kernel function as the classifier and choose a group of better kernel function parameters to analyze the classification performance of CMDSES and CMMF under the circumstances of different observation times, different PRFs,

Table 3. CCRs of CMDSES and CMMF.

	CMDSES		CMMF	
	Training samples	Testing samples	Training samples	Testing samples
Jet aircrafts	99.33%	99.67%	98.67%	98.33%
Propeller aircrafts	87.11%	86.22%	88.67%	86.22%
Helicopters	60.40%	59.20%	89.40%	84.60%
Average CCR	79.36%	78.64%	91.36%	88.48%

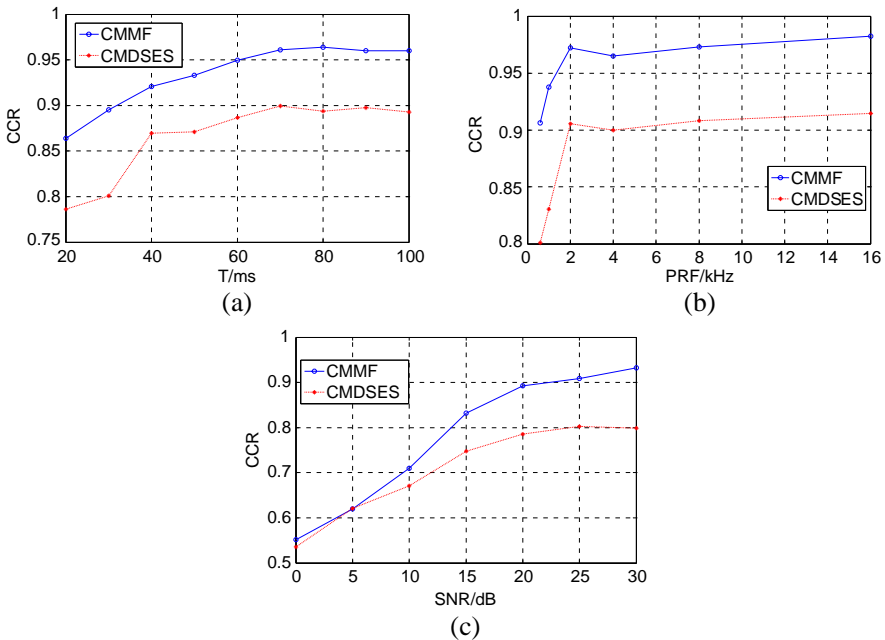


Figure 4. The variational curves of the average CCR with the observation time, PRF and SNR. (a) Observation time (L -band, PRF = 600 Hz, SNR = 20 dB) (b) PRF (L -band, $T = 25$ ms, SNR = 20 dB). (c) SNR (L -band, $T = 25$ ms, PRF = 600 Hz).

and different SNRs.

Figure 4 gives the variation curves of the average CCRs with the observation time, PRF, and SNR. It can be seen from the figure, corresponding to the conclusion in Experiment 1, CMMF outdoes CMDSES in the total performance under the same circumstances. In Figure 4(a), along with the increase of the observation time, the

calculated mass index curves and multifractal spectrum curves are able to reflect the difference consisting in the multifractal characteristics of return signals from different aircraft targets more adequately, so the average CCRs improve steadily. Moreover, the average CCRs of CMMF exceed those of CMDSES more than five percent with the same SNR. In Figure 4(b), under the circumstances of the radar operating at *L*-band, $T = 25$ ms, and $\text{SNR} = 20$ dB, the average CCRs of CMMF are all more than 90 percent. When PRF is greater than 2 kHz, the average CCRs change slowly, and the average CCR of CMMF exceeds that of CMDSES more than six percent with the same PRF. From Figure 4(c), we can see that both the average CCRs of the two methods are badly affected by SNR and improve steadily with the increase of SNR. When SNR is less than 5 dB, the average CCRs of the two methods are very close; however, when SNR is more than 10 dB, the average CCR of CMMF exceeds that of CMDSES more than four percent, and the difference between them will increase along with the farther increase of SNR. Moreover, what should be pointed out is that the data we used in the experiments are return signals from aircraft targets within a single observation. If we combine target echo data belonging to multiple observations, then the average CCR could still have a bigish increase.

5. CONCLUSIONS

The multifractal features of return signals from aircraft targets in conventional radars reveal the dynamic characteristics which induce the targets' echo structure, so they offer a new way for aircraft target classification and recognition by low-resolution surveillance radars. On basis of introducing the echo mathematic model of aircraft targets in conventional radars as well as the multifractal research methods, the paper sets out from the JEM modulation echo of aircraft targets and extracts the multifractal-feature-based JEM features, on this basis, puts forward a multifractal-feature-based target classification method with low-resolution radars. The experimental analysis shows that the multifractal features of return signals from three types of aircraft targets (including jet aircrafts, propeller aircrafts and helicopters) in conventional radar reveal their different nonlinear modulation characteristics, and the defined multifractal parameters can be used as effective features for aircraft target classification and recognition in the conventional radar. The experimental results also show that in the conventional low-resolution radar system with lower PRFs and shorter observation times, the multifractal-feature-based pattern classifier can classify the three types of aircraft targets effectively and has an

excellent classification performance in condition of no compensation for airframe components.

REFERENCES

1. Shirman, Y. D., *Computer Simulation of Aerial Target Radar Scattering, Recognition, Detection, and Tracking*, 111–124, Artech House, Boston, 2002.
2. Ding, J. J., *Target Recognition Techniques of Surveillance Radar*, 40–41, National Defense Industry Press, Beijing, 2008.
3. Chen, F., H. W. Liu, L. Du, et al., “Target classification with low-resolution radar based on dispersion situations of eigenvalue spectra,” *Science China: Information Sciences*, Vol. 53, 1446–1460, 2010.
4. Ghadaki, H. and R. Dizaji, “Target track classification for airport surveillance radar (ASR),” *Proceedings of IEEE Conference on Radar*, 24–27, 2006.
5. Leung, H., “Intelligent radar recognition system for surveillance,” *Proceedings of IEEE International Conference on Systems, Man and Cybernetics*, 2280–2285, 1995.
6. Leung, H. and J. Wu, “Bayesian and Dempster-Shafer target identification for radar surveillance,” *IEEE Transactions on Aerospace and Electronic Systems*, Vol. 36, 432–447, 2000.
7. Chan, S. C. and K. C. Lee, “Radar target identification by kernel principal component analysis on RCS,” *Journal of Electromagnetic Waves and Applications*, Vol. 26, No. 1, 64–74, 2012.
8. Pouliguen, P., L. Lucas, F. Muller, et al., “Calculation and analysis of electromagnetic scattering by helicopter rotating blades,” *IEEE Transactions on Antennas and Propagation*, Vol. 50, 1193–1408, 2002.
9. Bell, M. R. and R. A. Grubbs. “JEM modeling and measurement for radar target identification,” *IEEE Transactions on Aerospace and Electronic Systems*, Vol. 29, 73–87, 1993.
10. Piazza, E., “Radar signals analysis and modellization presence of JEM application in the civilian ATC radars,” *IEEE Aerospace and Electronic Systems Magazine*, Vol. 14, 35–40, 1999.
11. Martin, J. and B. Mulgrew, “Analysis of the theoretical return signal from aircraft blades,” *Proceedings of IEEE International Conference on Radar*, 569–572, 1990.
12. Yang, S. Y. and S. M. Yeh, “Electromagnetic backscattering

- from aircraft propeller blades,” *IEEE Transactions on Magnetics*, Vol. 33, 1432–1435, 1997.
13. Martin, J. and B. Mulgrew, “Analysis of the effects of blade pitch on the radar return signal from rotating aircraft blades,” *Proceedings of IET International Conference on Radar*, 446–449, 1992.
 14. Yoon, S., B. Kim, and Y. Kim, “Helicopter classification using time-frequency analysis,” *Electronics Letters*, Vol. 36, 1871–1872, 2000.
 15. Xian, M., Z. W. Zhuang, Z. P. Chen, et al., “The fractal characteristic of radar target based on polarimetry,” *Proceedings of the IEEE 1996 National Aerospace and Electronics Conference*, Vol. 1, 339–344, 1996.
 16. Mishra, A. K., H. Feng, and B. Mulgrew, “Fractal feature based radar signal classification,” *Proceedings of IET International Conference on Radar Systems*, 1–4, 2007.
 17. Ding, J. J. and X. D. Zhang, “Studies of analysis of JEM signatures and classification of targets in the conventional radar,” *Journal of Electronics and Information Technology*, Vol. 25 956–962, 2003.
 18. Elshafei, M., S. Akhtar, and M. S. Ahmed, “Parametric models for helicopter identification using ANN,” *IEEE Transactions on Aerospace and Electronic Systems*, Vol. 36, 1242–1252, 2000.
 19. Melendez, G. J. and S. B. Kesler, “Spectrum estimation by neural networks and their use for target classification by radar,” *Proceedings of IEEE International Conference on Acoustics, Speech, and Signal Processing*, 3615–3618, 1995.
 20. Moses, R. L. and J. W. Carl, “Autoregressive modeling of radar data with application to target identification,” *Proceedings of the 1988 IEEE National Radar Conference*, 220–224, 1988.
 21. Pellegrini, S. P. F. and C. S. Pardini, “Radar signals analysis oriented to target characterization applied to civilian ATC radar,” *Proceedings of IET International Conference Radar*, 438–445, 1992.
 22. Stove, A., “A Doppler-based target classifier using linear discriminants and principal components,” *Proceedings of IET Seminar on High Resolution Imaging and Target Classification*, 171–176, 2006.
 23. Jahangir, M., K. M. Ponting, and J. W. O’Loghlen, “Robust Doppler classification technique based on hidden Markov models,” *Proceedings of IEEE International Conference on Radar*, 162–166,

- 2002.
24. Jahangir, M., K. M. Ponting, and J. W. O'Loughlen, "Correction to robust Doppler classification technique based on hidden Markov models," *Proceedings of IEE International Conference on Radar, Sonar and Navigation*, Vol. 150, 387, 2003.
 25. Ji, H. B., J. Li, and W. X. Xie, "Bispectrum based radar target classification," *Proceedings of IEEE International Conference on Signal Processing*, 419–422, 1998.
 26. Grassberger, P., "Generalized dimensions of strange attractors," *Physics Letters A*, Vol. 97, 227–230, 1983.
 27. Hentschel, H. G. E. and I. Procaccia, "The infinite number of generalized dimensions of fractals and strange attractors," *Physica D*, Vol. 8, 435–444, 1983.
 28. Halsey, T. C., M. H. Jensen, et al., "Fractal measures and their singularities: The characterization of strange sets," *Physical Review A*, Vol. 33, 1141–1151, 1986.
 29. Telesca, L., V. Lapenna, and M. Macchiato, "Mono- and multi-fractal investigation of scaling properties in temporal patterns of seismic sequences," *Chaos, Solitons and Fractals*, Vol. 19, 1–15, 2004.
 30. Andric, M., Z. Durovic, and B. Zrnica, "Ground surveillance radar target classification based on fuzzy logic approach," *Proceedings of IEEE International Conference on Computer as a Tool*, Vol. 2, 1390–1392, 2005.
 31. Dullard, B. D. and P. C. Dowdy, "Pulse Doppler signature of a rotary wing aircraft," *IEEE Aerospace and Electronic Systems Magazine*, Vol. 36, 28–30, 1991.
 32. Yoon, S., B. Kim, and Y. Kim, "Helicopter classification using time-frequency analysis," *Electronics Letters*, Vol. 36, 1871–1872, 2000.
 33. Duda, R. O., P. E. Hart, and D. G. Stork, *Pattern Classification*, 259–264, 2nd Edition, John Wiley and Sons, New York, 2001.